Radiation-induced foil electret chamber

B. G. Fallone and E. B. Podgorsak
Departments of Radiation Oncology and Diagnostic Radiology, McGill University, 1650 avenue des Cèdres, Montréal, Québec H3G 1A4, Canada
(Received 22 February 1983; revised manuscript received 11 July 1983)

Saturation current densities, extrapolated electric fields, and electret-charging and -discharging current-density profiles in an ionization electret chamber are discussed as a function of various chamber parameters, such as air-gap and polymer thickness, polarizing electrode material, exposure rate, etc. Both the saturation current density and the extrapolated electric field consist of two components; one is linear with the air-gap thickness and is attributed to primary ionization in air, and the other exhibits exponential saturation and is attributed to air ionization caused by photoelectrons backscattered into the chamber sensitive volume from the polarizing electrode.

I. INTRODUCTION

Many techniques have been described for charging thin dielectric foils to form electrets. Originally, electrets were produced through thermal[1] (thermoelectrets) or optical[2] (photoelectrets) charge deposition methods; recently, however, isothermal charge deposition techniques have been favored because of their ease and speed[3–9]; the most popular is corona charging,[3,4] which uses an inhomogeneous electric field to produce a discharge in air at atmospheric pressure.

We have recently reported a new isothermal technique for forming electrets with uniform and stable charge densities of up to 10^{-6} C/cm^2.[10] X rays are used to produce, in air, free-charge carriers, which drift in an electric field and get trapped on a polymer foil to form an electret. The basic relationships governing the charging and discharging dynamics of this radiation-induced foil electret have been derived[11] using the laws of Gauss and Kirchoff, and the recently discovered hyperbolic relationship describing the saturation curves of parallel-plate ionization chambers.[12]

In this paper we discuss the dependence of the electret-charging and -discharging dynamics on the electret chamber parameters, such as polymer and air-gap thickness, polarizing electrode material, etc. The influence of these parameters on the chamber saturation current density and on the extrapolated electric field is also discussed.

II. EXPERIMENTAL

The electret forming chamber resembles a standard parallel-plate ionization chamber as shown schematically in Fig. 1. Various metals ranging from aluminum to lead were used as the conductive polarizing electrode. The measuring electrode was made of aluminum grounded through an electrometer, and blocked by a polymer foil with a typical thickness of 100 μm. The air gap was variable from 1 mm to a few cm. Both electrodes were circular with a diameter of 5 cm surrounded by a 1-cm wide guard ring.

The air at atmospheric pressure in the chamber-sensitive volume is ionized by electrons produced by the direct interactions of photons with air molecules and by photoelectrons which are produced by x rays in the polarizing electrode and backscattered into the chamber-sensitive volume. The free-charge carriers drift in the chamber's effective electric field towards the appropriate electrode. In contrast to a standard ionization chamber, where the charges impinge directly onto the electrodes, in the electret chamber the charges moving in the direction of the measuring electrode are stopped and trapped on the polymer surface to form a stable foil electret. The polarity of the electret depends on the direction of the externally applied electric field. The initial electret-charging current is proportional to the sensitive air volume and to the x-ray exposure rate. It also depends strongly on the atomic number of the polarizing electrode reflecting the photoemission contribution to the air ionization in the electret chamber sensitive volume.

The x rays were generated by a constant potential therapy unit (General Electric Company model no. Maximar-100) with a maximum potential of 100 kV (peak) and an anode current of 3 mA. The half-value layer of the x-ray beam was 2.2 mm of aluminum, corresponding to an effective x-ray beam energy of 28 keV. The polarizing electrode was at a distance of 50 cm from the target irrespective of air-gap thickness. The exposure rate at that distance from the target was 50 mR s^{-1} mA^{-1}.

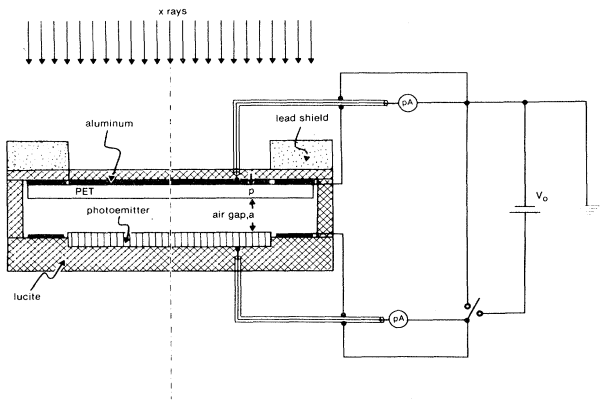

FIG. 1. Schematic diagram of the electret chamber.

 ©1983 The American Physical Society

III. RESULTS AND DISCUSSION

A. Electret-charging and -discharging characteristics

The current density $j(t)$ measured during the electret-charging or -discharging process is expressed as[11]:

$$j(t)=j_{\text{sat}}e^{(t_0-t)/\tau}(1+e^{2(t_0-t)/\tau})^{-1/2}\,, \tag{1}$$

where j_{sat} is the electret chamber saturation current density, and τ, the electret relaxation time, as well as t_0, the electret characteristic polarization or depolarization time, are given as follows

$$\tau=\epsilon_0(a\epsilon_p+p\epsilon_a)E^*/pj_{\text{sat}} \tag{2}$$

and

$$t_0=\tau\ln\sinh[E_a(0)/E^*]\,, \tag{3}$$

with a and p, the air-gap and polymer thickness, respectively, ϵ_a and ϵ_p the dielectric constants, E^* the electret chamber extrapolated electric field,[12] and $E_a(0)$ the applied electric field in the air gap.

In the saturation region, where $E_a(0)>3E^*$ and $t_0>\tau$, $j(t)$ exhibit the following behavior: At $t=0$ it is equal to j_{sat} and remains equal to j_{sat} until the effective field in the air gap falls below $3E^*$. Then $j(t)$ begins to decrease, becomes equal to $(1/\sqrt{2})j_{\text{sat}}$ at $t=t_0$, and exponentially approaches zero as t increases further.

The electret relaxation time τ is a function of both the electret chamber characteristics (air-gap, polymer thickness and type, polarizing electrode material) and the exposure rate of the x-ray beam. It does not, however, depend on the magnitude of the externally applied field $E_a(0)$.

The electret characteristic polarization time t_0, which is defined as the time in which $j(t)$ becomes equal to $(1/\sqrt{2})j_{\text{sat}}$, is directly proportional to τ but it also depends in a seemingly complicated manner on $E_a(0)$. For experiments in the saturation region, however, we may approximate Eq. (3) by

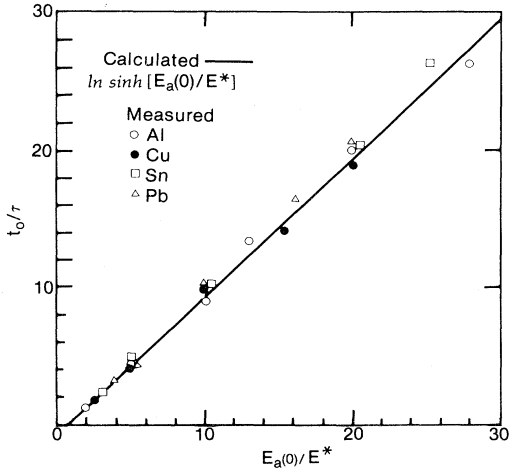

FIG. 2. Measured and calculated values for t_0/τ as a function of $E_a(0)/E^*$.

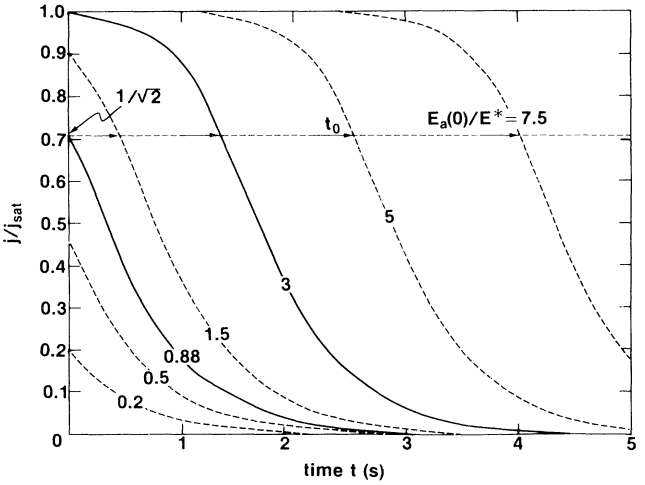

FIG. 3. Calculated polarization or depolarization current density j, normalized to j_{sat} for various $E_a(0)/E^*$ ranging from 0.2 to 7.5 ($\tau=0.59$ s).

$$\frac{t_0}{\tau}=\frac{E_a(0)}{E^*}-\ln 2\,, \tag{4}$$

which suggests that t_0/τ is linearly proportional to the applied field $E_a(0)$. In Fig. 2 we plot experimentally determined values of t_0/τ as a function of $E_a(0)/E^*$ for various polarizing electrode materials. The solid line represents a plot of Eq. (3) in excellent agreement with experimental data. The t_0/τ curve intercepts the abscissa at $E_a(0)/E^*=0.88$, which corresponds to $t_0=0$. The electret polarization current density is, from Eq. (1), for $t_0=0$, written as

$$j=j_{\text{sat}}e^{-t/\tau}(1+e^{-2t/\tau})^{-1/2}\,, \tag{5}$$

and exhibits a typical exponential decay starting at $j=(1/\sqrt{2})j_{\text{sat}}$ for $t=0$.

The electret characteristic polarization or depolarization time t_0 is thus a linear function of the applied field $E_a(0)$

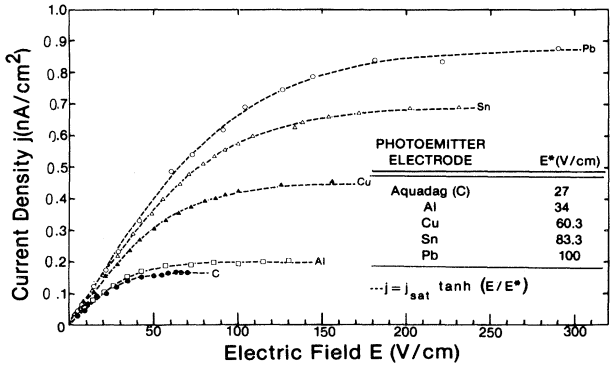

FIG. 4. Current density j as a function of the applied electric field E in an ionization chamber with an air gap a of 3.48 cm for various polarizing electrode materials. Exposure rate is 9 R/min. The dashed curves represent calculated saturation curves (Ref. 12) with the appropriate E^*.

for $E_a(0)/E^* > 3$ where the saturation condition prevails, and the initial electret polarization or depolarization current density $j(0)$ is equal to j_{sat}. In the region $0.88 \leq E_a(0)/E^* < 3$, the initial j(0) is between j_{sat} and $(1/\sqrt{2})j_{sat}$, j exponentially decays to zero, and t_0 is still defined by Eq. (3) as that time during the electret polarization or depolarization process in which the current drops to $(1/\sqrt{2})j_{sat}$. For $0 < E_a(0)/E^* < 0.88$, the initial $j(0)$ is smaller than $(1/\sqrt{2})j_{sat}$, $t_0 < 0$, and $j(t)$ rapidly decays to zero. In Fig. 3 we show examples of polarization current-density profiles calculated from Eq. (1) for various values of $E_a(0)/E^*$.

B. Saturation current density in the electret chamber

Equation (1) gives the general shape of the radiation induced electret-charging or -discharging current-density profile, depending strongly on the saturation current density j_{sat} and the extrapolated electric field E^*. In order to study the behavior of j_{sat} and E^*, we converted the electret chamber into a standard parallel-plate ionization chamber and measured saturation curves for various polarizing electrode materials and air gaps. As shown in Fig. 4, for a given air-gap and exposure rate, j_{sat} depends strongly on the atomic number Z of the polarizing electrode, exhibiting an almost fivefold increase when aluminum is replaced by lead. The dashed curves represent current densities calculated from the relationship[12]

$$j = j_{sat} \tanh(E/E^*) , \tag{6}$$

with the use of experimentally determined values for E^*. The agreement between measured and calculated saturation curves is excellent.

In Fig. 5 we plot j_{sat} (solid curves) as a function of a for various polarizing electrode materials. For a given material j_{sat} increases linearly with a for large a; for small a, however, the linearity breaks down. The j_{sat} vs a curve may be separated into two components as

$$j_{sat}(a) = j_{sat}^{air}(a) + j_{sat}^{p}(a) , \tag{7}$$

where the linear function j_{sat}^{air} is produced by charge carriers originating from electrons released in the chamber-sensitive volume by direct interactions of photons with air molecules, and the exponential function j_{sat}^{p} is produced by the photoelectrons backscattered from the polarizing electrode into the chamber-sensitive volume. These photoelectrons have a range a_r of ~ 1 cm for our x-ray photon energy at atmospheric pressure.[13]

The linear function j_{sat}^{air} is independent of the electrode material and linearly dependent upon the air gap a and the exposure rate $\dot{X}$

$$j_{sat}^{air} = \kappa a \dot{X} , \tag{8}$$

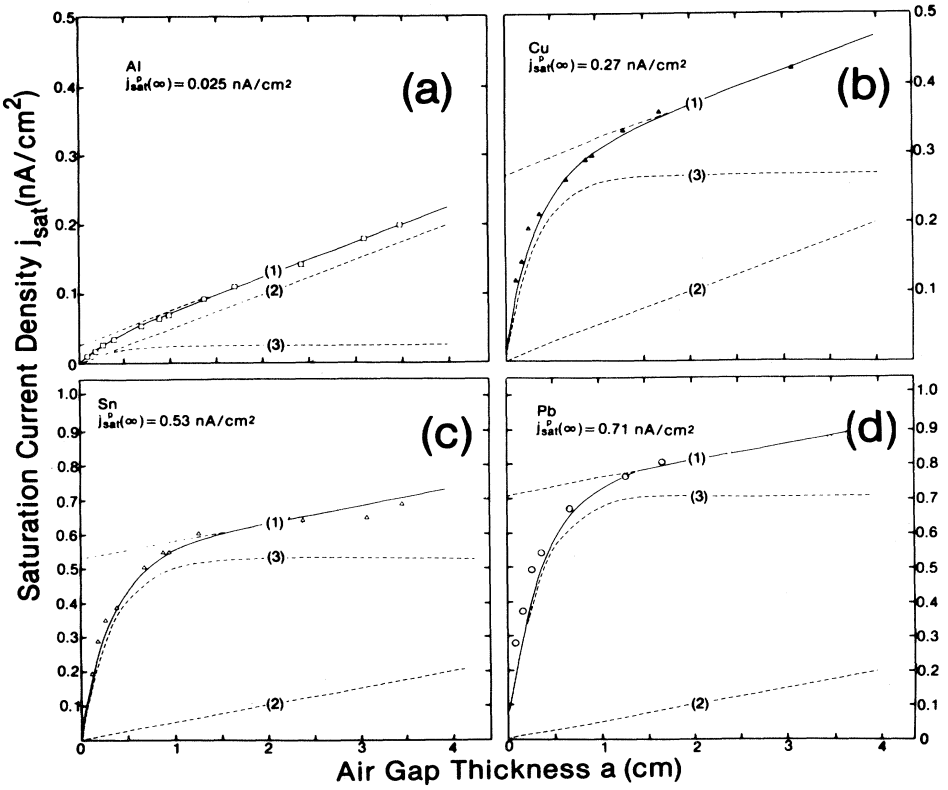

FIG. 5. Saturation current density j_{sat} as a function of air gap a for various electrode materials. Exposure rate is 9 R/min. Curves (1) represent a plot of Eq. (11), curves (2) represent Eq. (8), and curves (3) represent Eq. (9).

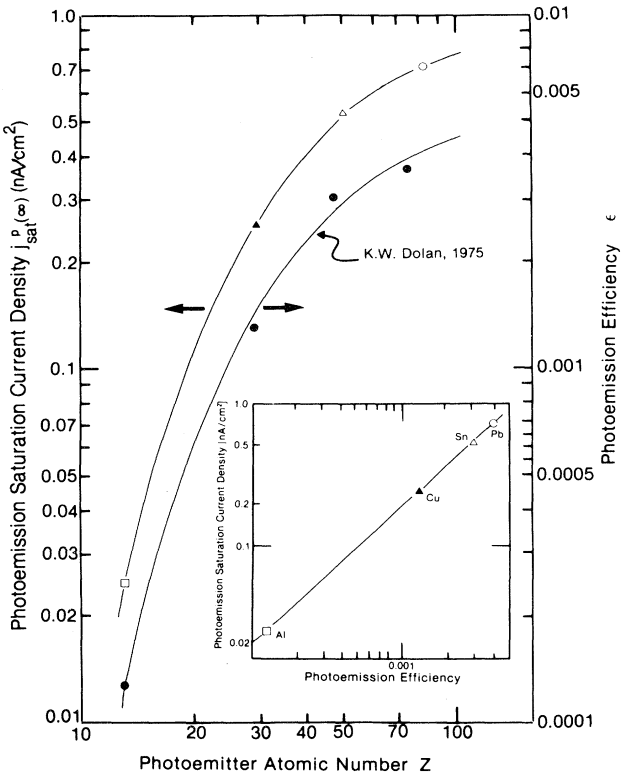

FIG. 6. Photoemission saturation current density $j^p_{sat}(\infty)$ and photoemission efficiency ϵ (Ref. 13) as a function of polarizing electrode atomic number. The inset shows direct proportionality between $j^p_{sat}(\infty)$ and ϵ.

where κ is the usual proportionality constant 3.33×10^{-10} As/cm^{3}R. Equation (8) is plotted in Fig. 5 as dashed lines (2) for an exposure rate of 9 R/min. Note that j^{air}_{sat} is identical for all electrode materials.

Empirically, we find that $j^p_{sat}(a)$, represented as curves (3) in Fig. 5, may be expressed as follows:

$$j^p_{sat}(a)=j^p_{sat}(\infty)(1-e^{-3a/a_r}) , \tag{9}$$

where $j^p_{sat}(\infty)$, the photoemission saturation current density for $a\gg a_r$, is obtained by extrapolating the measured linear portion of $j_{sat}(a)$ to $a=0$.

The relationship between $j^p_{sat}(\infty)$ and the efficiency $\epsilon(Z,E_\nu)$ for production of backscattered electrons, defined[13] as the number of backscattered electrons per incident photon of energy E_ν, is shown in Fig. 6 for various electrode materials Z. The inset shows direct proportionality between $j^p_{sat}(\infty)$ and the values for $\epsilon(Z,E_\nu)$, i.e.,

$$j^p_{sat}(\infty)=\lambda\epsilon(Z,E_\nu)=\lambda'\dot{\chi}\epsilon(Z,E_\nu) , \tag{10}$$

where λ is an exposure-rate-dependent proportionality constant, and λ' is a proportionality constant independent of the exposure rate and empirically found equal to 1.33×10^{-6} (C/R cm^2) (electrons/photon)$^{-1}$.

The saturation current density j_{sat} may thus in general be expressed as

$$j_{sat}(a,Z,E_\nu)=\dot{\chi}[\kappa a+\lambda'\epsilon(Z,E_\nu)(1-e^{-3a/a_r(E_\nu)})] , \tag{11}$$

where κ and λ' are constants given above, $\epsilon(Z,E_\nu)$ is the efficiency for production of backscattered photoelectrons, and $a_r(E_\nu)$ is the range of photoelectrons in air at normal temperature and pressure.

In standard ionization chambers, where low atomic number materials are used as the polarizing electrode, $\epsilon(Z,E_\nu)$ is so small that the photoemission term of j_{sat} is negligible in comparison with primary air ionization. With lead as polarizing electrode material, on the other hand, the main contribution to j_{sat} comes from the photoemission term because of the large value of $\epsilon(Z,E_\nu)$ for lead.

C. Extrapolated electric field

The extrapolated electric field E^* is a parameter in the saturation curve expression, depending on the configuration of the parallel-plate ionization chamber and the x-ray exposure rate. In Fig. 7 we show E^* as a function of air-gap thickness a for various polarizing electrode materials. Similarly, to the j_{sat} vs a behavior, $E^*(a)$ also has two components; one, $E^*_{air}(a)$, is linear for all a and is again attributed to primary ionization in air, and the other, $E^*_p(a)$ exhibits an exponential saturation behavior at approximately $3a_r$ and is attributed to the photoemission from the polarizing electrode. The saturation value, $E^*_p(\infty)$, is obtained by extrapolating the linear portion of the E^* vs a curve to $a=0$. We have shown recently[12] that $E^*_{air}(a)$, represented in Fig. 7 by curves (2), may be expressed as

$$E^*_{air}(a)=k(aj^{air}_{sat})^{1/2}=k\sqrt{\kappa}a\dot{\chi}^{1/2} , \tag{12}$$

where k is a universal parallel-plate ionization chamber constant equal to 12.4×10^5 V/(A cm)$^{1/2}$, and κ was defined above.

The subtraction of $E^*_{air}(a)$ from $E^*(a)$ yields $E^*_p(a)$ shown as curves (3) in Fig. 7. Empirically we find that $E^*_p(a)$ may be expressed, similarly to $j^p_{sat}(a)$, by an exponential expression

$$E^*_p(a)=E^*_p(\infty)(1-e^{-a/a_r}) . \tag{13}$$

In Fig. 8 we plot $E^*_p(\infty)$ for various photoemitter materials as a function: (a) of photoemitter atomic number Z, showing a strong Z dependence of $E^*_p(\infty)$, (b) of photoemission saturation current density $j^p_{sat}(\infty)$, showing direct proportionality between $E^*_p(\infty)$ and $j^p_{sat}(\infty)$, and (c) of photoemission efficiency $\epsilon(Z,E_\nu)$, showing a linear relationship between $E^*_p(\infty)$ and $\epsilon(Z,E_\nu)$.

In general, $E^*_p(\infty)$ may thus be expressed, incorporating Eq. (10), as

$$E^*_p(\infty)=mj^p_{sat}(\infty)=m\lambda'\dot{\chi}\epsilon(Z,E_\nu) , \tag{14}$$

where m is the slope from Fig. 8(b) and λ' was defined in

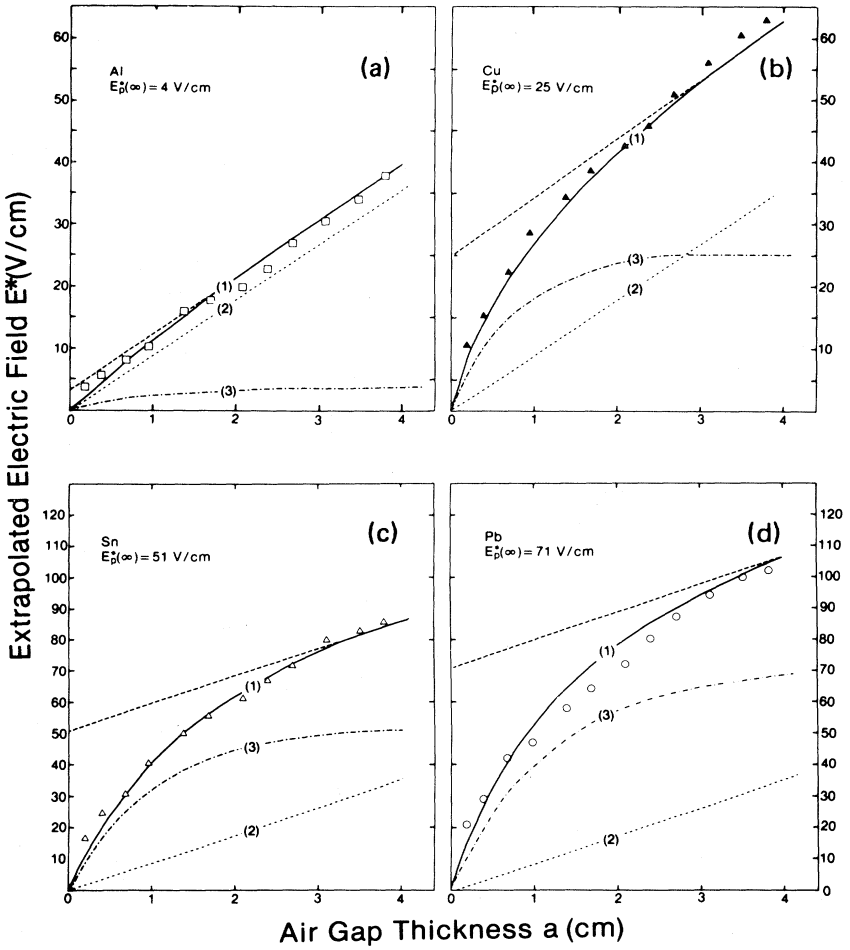

FIG. 7. Extrapolated electric field E^* as a function of polarizing electrode materials. Exposure rate is 9 R/min. Curves (1) represent Eq. (15), curves (2) Eq. (12), and curves (3) represent Eq. (13).

the preceding section.

The general relationship for the extrapolated field $E^*(a,Z,E_v)$ is now given by

$$E^*(a,Z,E_v)=k'a\dot{\chi}^{1/2}+m'\epsilon(Z,E_v)\dot{\chi} \times(1-e^{-a/a_r(E_v)}), \quad (15)$$

where $m'=m\lambda'=1.33\times10^5$ V cm^{-1} (R/s)$^{-1}$ (electrons/photon)$^{-1}$, and $k'=k\sqrt{\kappa}=22.6$ V cm^{-2}(R/s)$^{-1/2}$. The extrapolated field E^* thus consists of two terms: one, determined by the primary ionization in air, is dominant for chambers with low atomic number electrodes, and the other, determined by photoemission from the polarizing electrode, is dominant at high atomic number polarizing electrodes.

D. Polarization current-density profiles

The time dependence of the electret polarization current density during the electret-charging process is described by Eq. (1). In this section we discuss the general properties of polarization current-density profiles based on the saturation current density j_{sat} and extrapolated field E^*. In Figs. 9 and 10 we show various calculated polarization current-density profiles obtained in the electret chamber with a lead polarizing electrode and with various air gaps a ranging from 0.18 to 3.48 cm for an applied field $E_a(0)$ equal to $5E^*$ (Fig. 9) and a constant applied voltage V_0 of 500 V (Fig. 10). The insets to both figures give relevant parameters, such as E^*, $E_a(0)$, and j_{sat} as a function of a. The extrapolated fields E^* were obtained from measured saturation curves for various air gaps and agree well with data calculated from Eq. (15). The electret relaxation times τ and characteristic polarization times t_0 were calculated from Eqs. (2) and (3), respectively.

The condition $E_a(0)=5E^*$ in Fig. 9 ensures that the electret chamber is initially in the saturation region for all air gaps and the initial polarization current density is equal to the standard saturation current density j_{sat}. A plot of measured $j_{sat}(a)$ for a lead electrode was shown in Fig. 5(d) in excellent agreement with data calculated from Eq. (11). Combining Eqs. (2) and (4) we get

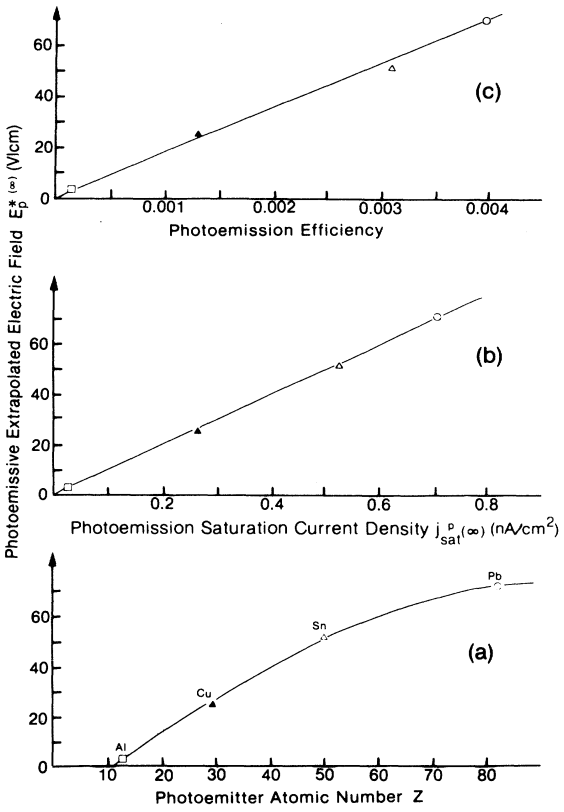

FIG. 8. Photoemissive extrapolated electric field $E_p^*(\infty)$ as a function (a) of polarizing electrode atomic number Z, (b) of photoemission saturation current density $j_{sat}^p(\infty)$, and (c) of photoemission efficiency.

$$t_0=\frac{\epsilon_0(a\epsilon_p+p\epsilon_a)E^*}{pj_{sat}}\left[\frac{E_a(0)}{E^*}-\ln 2\right], \tag{16}$$

the characteristic electret polarization time, which at least for small air gaps gives a fairly good indication of the time needed to charge the electret to its maximum charge density σ_{max}. At larger gaps, however, the current profile becomes less and less steep and the time needed to fully charge the electret is much longer than t_0, which is still defined as the time where $j=(1/\sqrt{2})j_{sat}$.

Figure 10 shows polarization current-density profiles for a constant external voltage V_0 of 500 V applied across air gaps of various thicknesses. The chamber is in the saturation region for the three small air gaps since for them $E_a(0)>3E^*$. The current profiles start at j_{sat}, remain constant for a while depending on t_0, and then exponentially drop to zero. The areas under all three profiles are identical and equal to the maximum surface charge density. For the air gaps of 2.38 and 3.48 cm, however, the chamber is not in the saturation region, the initial current density is lower than j_{sat} and starts an immediate decay towards zero. The areas under the current profiles, however, are also equal to σ_{max}, indicating that the electret becomes fully charged even in situations where saturation conditions do not prevail in the electret chamber. It is evident from Fig. 10 that the time required to fully charge the electret under these conditions can become quite large.

In Fig. 11 we compare the calculated [Eq. (1)] and measured polarization current profiles for various polarizing electrode materials, for an air gap of 0.18 cm and for three

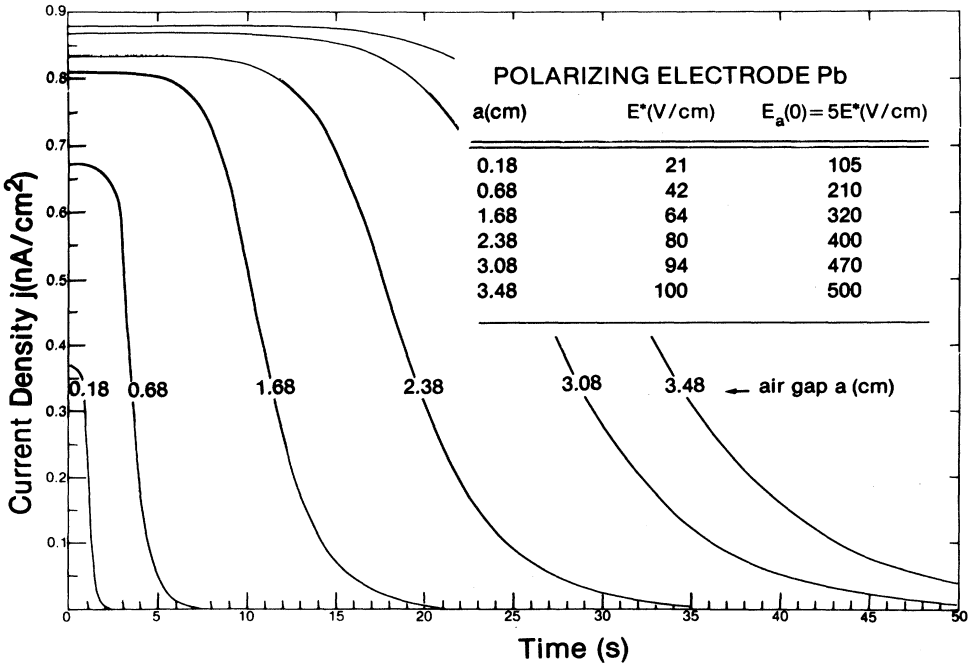

FIG. 9. Calculated time dependence of the electret-charging or -discharging current j for a lead polarizing electrode with various air gaps a. The electret chamber was initially under saturation conditions since $E_a(0)=5E^*$ for all a.

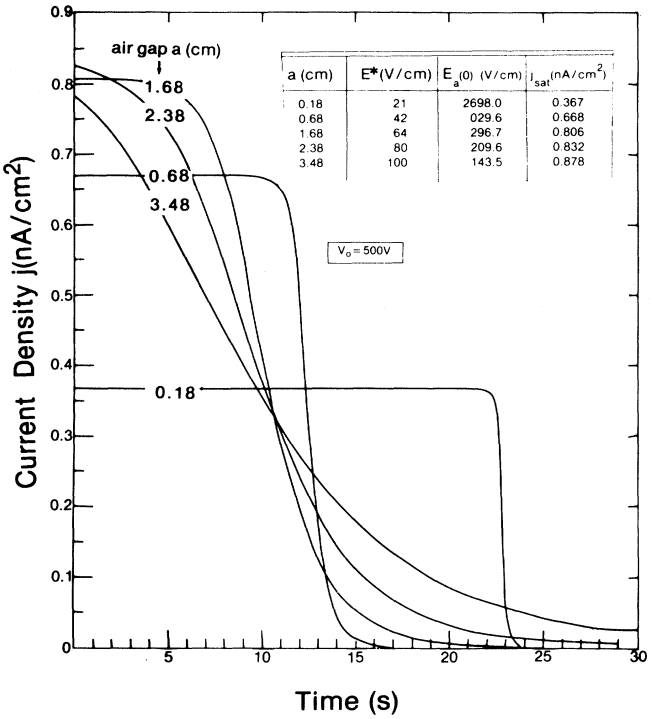

FIG. 10. Calculated time dependence of the electret-charging or -discharging current j for a lead polarizing electrode with various air gaps a. The externally applied voltage V_0 was 500 V for all air gaps.

applied fields $E_a(0)$ equal to approximately $5E^*$, $10E^*$, and $20E^*$. We notice that for $E_a(0) \sim 5E^*$ the agreement between calculated and measured profiles is excellent; for large applied fields, however, the calculated curve is considerably steeper than the measured one. This discrepancy may be attributed to the electret chamber, where a breakdown in saturation characteristics may occur at very high voltages, or to the electret-charging characteristics which may depend on charge densities already trapped on the polymer surface.

IV. CONCLUSION

A new isothermal technique for production of stable foil electrets has been developed recently. X rays are used to create free charges which are subsequently trapped on a polymer foil to form the electret. The apparatus closely resembles a parallel-plate ionization chamber used in radiation dosimetry. The measured electret-charging and -discharging current-density profiles agree well with profiles calculated using the laws of Gauss and Kirchoff in conjunction with the recently discovered hyperbolic relationship describing the saturation curves of parallel-plate ionization chambers. The profiles are given in terms of the electret chamber saturation current density and of the extrapolated electric field, both depending on the chamber physical parameters, such as air-gap and polymer thickness, polarizing electrode material, x-ray exposure rate, etc. General relationships for the saturation current density and the extrapolated field were given, showing that

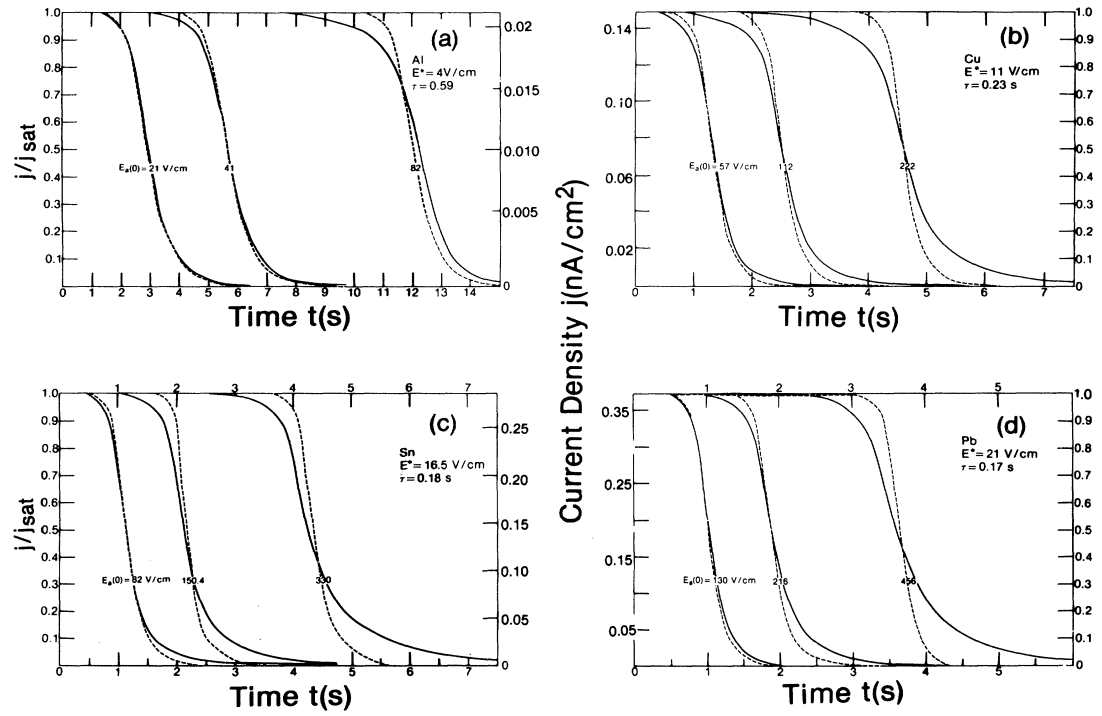

FIG. 11. Theoretical (dashed) vs measured (solid) polarization current densities as a function of time for various polarizing electrode materials and externally applied fields $E_a(0)$. The air-gap thickness a was 0.18 cm, exposure rate 9 R/min.

the two consist of two components, one linear with the air-gap thickness and attributed to primary ionization in air, and the other exhibiting an exponential saturation and attributed to air ionization caused by photoelectrons backscattered into the chamber sensitive volume from the polarizing electrode.

ACKNOWLEDGMENTS

We would like to thank Dr. Richard Heese for helpful discussions. This work was supported in part by the Medical Research Council of Canada under Grant No. MA-6960.

[1]*Electrets,* Vol. 33 of *Topics in Applied Physics,* edited by G. M. Sessler (Springer, Berlin, 1980).

[2]V. M. Fridkin and I. S. Zheludev, in *Photoelectrets and the Electrophotographic Process* (Consultants Bureau, New York, 1960).

[3]C. F. Carlson, U. S. Patent No. 2 588 699 (1952).

[4]R. M. Schaffert, *Electrophotography,* (Focal, London, 1975).

[5]G. M. Sessler and J. E. West, J. Appl. Phys. 43, 922 (1972).

[6]P. W. Chudleigh, J. Appl. Phys. 47, 4475 (1976).

[7]B. Gross, G. M. Sessler, and J. E. West, J. Appl. Phys. 45, 111 (1975).

[8]G. M. Sessler and J. E. West, J. Electrostatics 1, 111 (1975).

[9]B. Gross, G. M. Sessler, and J. E. West, J. Appl. Phys. 47, 968 (1976).

[10]B. G. Fallone and E. B. Podgorsak, Phys. Rev. B 27, 2615 (1983).

[11]B. G. Fallone and E. B. Podgorsak, Phys. Rev. B 27, 5062 (1983).

[12]B. G. Fallone and E. B. Podgorsak, Med. Phys. 10, 191 (1983).

[13]K. W. Dolan, J. Appl. Phys. 46, 2456 (1975).